Final Technical Report

Date of Final Report: August 31, 2006
EPA Grant Number: R827352C015
Center Name: Southern California Particle Center and Supersite (SCPCS)
Center Director: John R. Froines
Title: Exposure Assessment and Airshed Modeling Applications in Support of SCPC and CHS Projects
Investigators: Richard P. Turco, Arthur M. Winer, Frederick W. Lurmann, Rong Lu, Jun Wu
Institution: University of California–Los Angeles
EPA Project Officer: Stacey Katz/Gail Robarge
Project Period: June 1, 1999–May 31, 2005 (no-cost extension to May 31, 2006)
Period Covered by the Report: June 1, 1999–May 31, 2006
RFA: Airborne Particulate Matter (PM) Centers (1999)
Research Category: Particulate Matter

Topic C: Studies of the Effects of Varying Spatial and Temporal Patterns of Ambient Particulate Matter (PM) and Co-pollutants and Resulting Health Effects with Emphasis on the Role of Atmospheric Chemistry

Objective(s) of the Research Project: Two overall objectives of this integrated modeling project were to utilize airshed model outputs as inputs to exposure assessment models designed to quantify long-term average exposure of subjects in the Children's Health Study (CHS) to criteria pollutants; and assess population exposure to ambient naphthalene concentrations in Southern California. In the course of this research we also demonstrated significant problems with the accuracy of widely-used roadway networks and geocoded addresses. In addition, we developed methods for improvements in these important parameters, and also investigated environmental justice implications of traffic-related air pollution in Southern California.

The major elements of this final report are:

1. Exposure Assessment

    a. Exposure assessment for the CHS Children
    b. Naphthalene exposure assessment for the population of Southern California
    c. Improving spatial accuracy of roadway network and geocoded addresses
    d. Environmental justice and traffic-related pollution in Southern California

2. Airshed Modeling

    a. Regional distributions and behavior of particulate-borne trace metals in the Los Angeles Basin (LAB)
    b. Properties of diesel exhaust in the LAB: elemental carbon sources and distributions
    c. Distributions of Naphthalene and its derivative quinones in the LAB
    d. Application of the SMOG model in support of the SCPC CHS

e. Modeling ultrafine particles (UF) near major roadways for human exposure assessment

Summary of Findings:

Exposure Assessment for the CHS Children

Objectives. The overall objective of this modeling study was to provide, retrospectively, more accurate and comprehensive assessments of the long-term average exposure of the individual children in the CHS to vehicle-related pollutants. The specific objectives of the present study were to quantify the variability of within-community exposures; to determine exposures due to local mobile source emissions (LMSE) relative to meteorologically-transported pollutants and local non-mobile source emissions (LN-MSE); and to facilitate evaluation of relationships between exposure and health outcomes for the individual children in the CHS cohort.

Project Summary. We developed an Individual Exposure Model (IEM) to retrospectively estimate the long-term average exposure of the individual CHS children to vehicle-related pollutants, including CO, NO_2, PM_{10}, $PM_{2.5}$, and elemental carbon ($PM_{2.5}$ portion). Exposures were estimated by tracking children's time-activity in five microenvironments (residential outdoor, residential indoor, school outdoor, school indoor, and in vehicle) where children spend most of their time. A time-activity submodel was developed to create 24-hr time-activity series for each child in the CHS cohort by using information from both the CHS survey and the Consolidated Human Activity Database (CHAD) developed by the U.S. Environmental Protection Agency (EPA). The CHS children were grouped by age, gender, day-type, time outdoors and time-in-vehicles. For each CHS category a child was grouped into, the corresponding CHAD distribution was sampled.

In the IEM, pollutant concentrations due to both local mobile source emissions and meteorologically-transported pollutants were taken into account by combining a line source model (CALINE4) with the Surface Meteorology and Ozone Generation (SMOG) model. To avoid double counting, local mobile sources were removed from SMOG and added back by CALINE4. The basis for this approach is that vehicle-related primary pollutant concentrations can be separated into, and modeled as local mobile source emissions, and transported and local non-mobile source emissions. Indoor pollutant concentrations were estimated from a single-compartment, steady-state mass balance equation, through which contributions from indoor and outdoor sources were separated. In-vehicle pollutant concentrations were estimated based on recent in-vehicle and in-bus measurements conducted in California. Pollutant exposures due to outdoor origins were estimated for seven CHS communities in the California South Coast Air Basin (SoCAB), including Lancaster (LAN), San Dimas (SDM), Upland (UPL), Mira Loma (MRL), Riverside (RIV), Long Beach (LGB), and Lake Elsinore (LKE).

The study showed that the ratio of pollutant concentrations from transport and local non-mobile sources was correlated inversely with traffic density. Most PM_{10} and $PM_{2.5}$ came from transport and local non-mobile source emissions, in agreement with recent studies showing that PM_{10} and $PM_{2.5}$ act more like regional pollutants rather than reflecting direct emissions from motor sources. Transported CO (including mobile source emissions from upwind locations) and LN-

MSE comprised over 60% of the CO concentrations at all of the CHS communities except Lancaster.

Model simulations were conducted for three scenarios: with local traffic adjustment and time-activity simulation (total exposure estimated using combined local and transported pollutant concentrations); without local traffic adjustment but with time-activity simulation (total exposure estimated using air monitoring station data); and without local traffic adjustment or time-activity simulation (annual average ambient concentrations). Personal PM_{10} exposures estimated for these three scenarios is plotted in Figure 1. We found local traffic significantly increased within-community variability for exposure to CO, NO_2, and PM-associated pollutants, especially at communities with heavy traffic (e.g. Long Beach). The overall within-community variability of personal exposures (including local traffic effects and time-activity differences) were highest for NO_2 (±20–40%), followed by EC (±17–27%), PM_{10} (± 15–25%), $PM_{2.5}$ (±15–20%), and CO (±9–14%), where the ranges are across seven CHS communities. Local traffic alone contributed most to CO and NO_2 exposures, but less to PM-related exposures. Significant within-community variability due to children's time-activity patterns was also observed, with the highest for NO_2 (±18–25%), followed by EC (±16–20%), PM_{10} (± 12–18%), $PM_{2.5}$ (±10–15%), and CO (±3–9%).

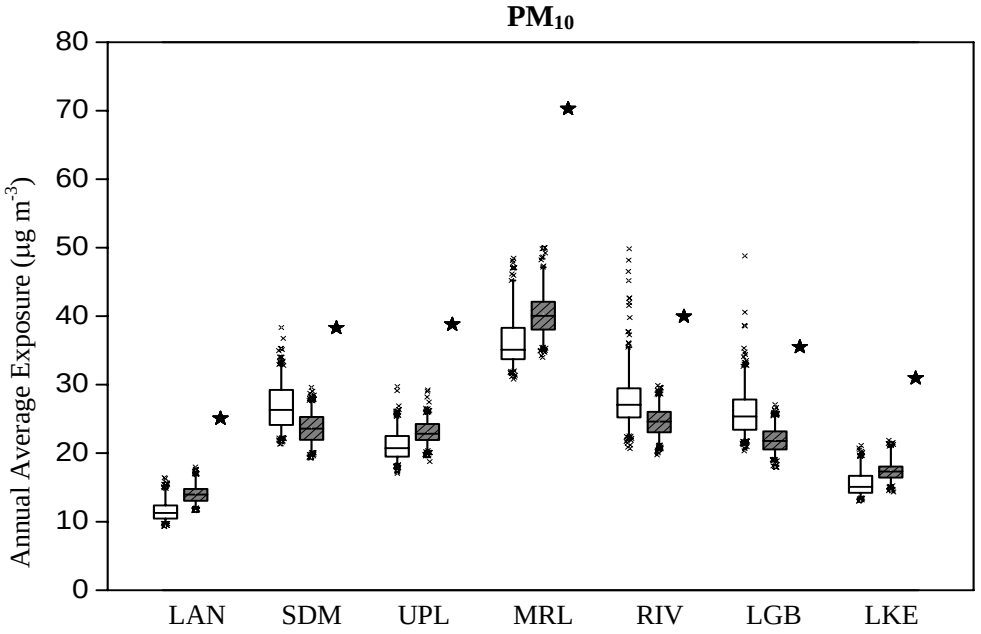

Figure 1. Estimated Annual Average Exposures of the CHS Children in 1997 Under Three Scenarios

Total exposure calculated using combined local and transported pollutant concentrations
Total Exposure calculated using monitoring station data; annual average ambient concentrations

Differences in community mean exposures were impacted by community location (e.g., source vs. receptor areas), traffic density, locations of residences and schools within a community. For

CO, the community mean personal exposure ranked RIV (1.8) > LGB (1.7) > SDM (1.5) > MRL (1.0) > LAN (0.7) (community mean exposure in mg m^{-3}). For PM_{10}, the community mean exposure ranked MRL (36.4) > RIV (28.0) > SDM (26.8) > LGB (26.1) > UPL (21.1) > LKE (15.7) > LAN (11.6) (in $\mu g\ m^{-3}$).

Conclusion. Local traffic significantly increased within-community variability for exposure to CO, NO_2, and PM-associated pollutants, especially in communities with heavy traffic. Exposures to PM-associated pollutants were impacted more by transport and local non-mobile source emissions. Significant within-community variability due to time-activity pattern differences was observed. Between-community exposure differences were affected by community location, traffic density, locations of residences and schools, and time-activity patterns of the children in each community. The ambient pollutant concentrations measured by the CHS central monitoring stations did a reasonable job of capturing the range of residence and school outdoor concentrations at Lancaster, Lake Elsinore, Upland, and Mira Loma, but not at San Dimas, Riverside, and Long Beach. This monitoring station "siting" issue has implications for epidemiological studies since many of these studies use ambient concentrations as surrogates for personal exposures.

Naphthalene Exposure Assessment for the Population of Southern California

Objectives. Naphthalene, a hazardous air pollutant and a potential carcinogen, can irritate the eyes, skin and respiratory tract, cause kidney and liver damage, and attack the central nervous system (USEPA, 2003). No exposure assessment has been conducted for the present SoCAB population due to extremely limited measurement data. The objective of this study was to estimate naphthalene exposure for the SoCAB population by applying a sophisticated air quality model and a human exposure model.

Project Summary. We linked the SMOG airshed model and the Regional Human Exposure (REHEX) model to assess human exposure to air pollutants in the SoCAB. Hourly ambient naphthalene concentrations predicted by the SMOG model were fed into the REHEX model as outdoor pollutant concentrations at a 5-kilometer resolution. Ratios of indoor-to-outdoor (I/O) naphthalene concentrations were obtained from the Fresno Asthmatic Children's Environment Study (FACES) in California, in which 150 naphthalene samples were collected inside and outside 47 non-smoker homes from 2002 to 2003. In the absence of any in-vehicle naphthalene measurements for the SoCAB, an average in-vehicle-to-ambient naphthalene ratio of three was assumed for this exposure assessment. Time-activity patterns for California residents were obtained from the CHAD.

Results showed mean hourly naphthalene exposures of 270 ng m^{-3} and 430 ng m^{-3} for the SoCAB population in the summer and winter episodes, respectively. These mean hourly exposures were about 80% higher than the population-weighted outdoor concentrations (150 ng m^{-3} and 230 ng m^{-3}) because of indoor sources and in-vehicle exposures. More than one million people in the SoCAB were exposed to naphthalene at mean concentrations exceeding 1000 ng m^{-3} during the winter period. Remarkably, about 65,000 and 1,300 people experienced naphthalene exposures exceeding 2000 ng m^{-3} and 3000 ng m^{-3} respectively, in the winter case.

Population naphthalene exposures correlated strongly with transportation corridors in the SoCAB since gasoline and diesel products and motor vehicle exhaust contribute more than half of the total emissions in the basin. High naphthalene exposures appeared in areas where both emissions and population densities were great, such as the downtown Los Angeles area. In addition, naphthalene exposures showed a high degree of regional-scale variability, from less than 50 ng m^{-3} to up to 1300 ng m^{-3} in 5-km grids, indicating that more than single-point sampling is required to characterize properly naphthalene and other polycyclic aromatic hydrocarbons (PAHs) in an urbanized region.

Indoor sources and travel by vehicles accounted for 40% and 4% of the total exposure, respectively. Exposure due to environmental tobacco smoke (ETS) was 5–14 ng m^{-3}, which accounted for only 1–5% of the total exposures, indicating that ETS is not a significant source of population naphthalene exposure, at least for the SoCAB population where smoking rates have declined significantly in recent years. However, we did not calculate naphthalene exposures due to direct smoking activities of single individual smokers, whose exposure to naphthalene while smoking would be significantly higher.

Conclusion. By linking the SMOG and REHEX models, we obtained the first comprehensive quantitative assessment of the population exposure to naphthalene in the SoCAB . Average hourly naphthalene exposures in the SoCAB under summer and winter conditions were 270 ng m^{-3} and 430 ng m^{-3}, respectively. Certain individuals experience much higher concentrations of naphthalene. More than one million and one thousand individuals were estimated to experience naphthalene exposure greater than 1000 and 3000 ng m^{-3}, respectively. Substantial spatial and temporal variations exist for naphthalene exposures, with populations living, working, or attending school adjacent to major roadways experiencing the highest exposures. Indoor sources and travel by vehicles accounted for 40% and 4% of the total exposure, respectively, while ETS accounted for less than 5% of total naphthalene exposures. The highest naphthalene exposures estimated from this modeling study exceed the reference concentration for chronic inhalation exposure adapted by the U.S. EPA (3000 ng m^{-3}).

Improving Spatial Accuracy of Roadway Networks and Geocoded Addresses

Objectives. Recent field studies indicate the highest exposures to direct vehicle-related pollutants are highly localized (within a few hundred meters) near major roadways (Hitchins, et al., 2000; Zhu, et al., 2002a; 2002b), suggesting a high spatial resolution, down to tens of meters, may be required to better characterize exposure to motor vehicle-related pollutants. Two main concerns arise when conducting exposure assessment studies on vehicle-related pollutants: 1) accurately mapping (geocoding) the residence locations of study participants; and 2) accurately mapping and characterizing road networks and traffic activity. The objectives of this study were to develop GIS-based methods to improve the accuracy of roadway network data associated with traffic activities; provide the optimum geocoding data available; assess the magnitude of potential exposure errors associated with spatially inaccurate roadways and misplaced addresses; and provide refined exposure assessment of vehicle-related pollutants to support the CHS.

Project Summary. We obtained vehicle activity data for southern California from the California Department of Transportation (Caltrans). The TeleAtlas MultiNet™ USA (TAMN) database

was also obtained since it had detailed roadway and address attribute information, a high degree of positional accuracy, and geocoding capability. The Caltrans roadways were based on United States Geological Survey (USGS) data with traffic activity data; while the TAMN roadways were based on global positioning system (GPS) validation but lacking traffic information.

Results showed that in highly urbanized areas there was generally good agreement between the spatial positioning of the Caltrans road network and the TAMN data, however, for some urban areas and several suburban areas, differences on the order of 50 m to 400 m were identified between the two datasets (Figure 2). In Los Angeles County, average discrepancies between the matched Caltrans and TAMN roadway segments were 21 m, 30 m, and 32 m for freeways, major roadways, and minor roadways, respectively. However, the actual difference between unmatched roadway segments could be much larger and more difficult to quantify.

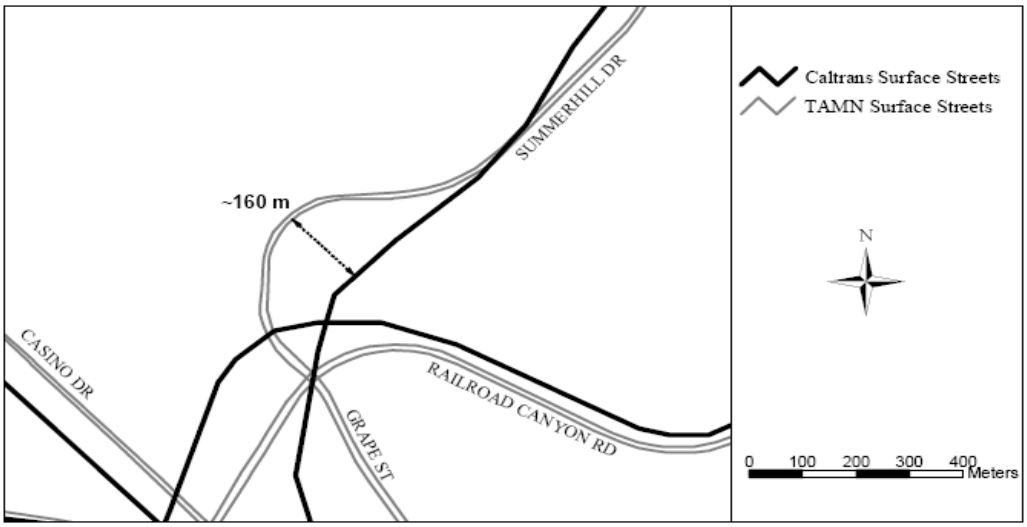

Figure 2. Comparison Between Caltrans and TAMN Roadway Network for Surface Streets in Riverside, CA, Showing Discrepancies Up to ~160 m

TeleAtlas geocoding service was used to locate 8,593 addresses. Ninety-seven percent of addresses were matched to an exact house number to the correct side of the street or unique intersection. Two percent of the addresses were located to the correct block but with unknown position along the block, which occurred most often in the rural communities of Lake Arrowhead, Alpine, and Lompoc or when an address was part of a large apartment complex. These addresses were manually corrected in 90% of cases, using aerial photography from the USGS Terraserver, MapQuest, Yahoo, and the USPS Zip4 website. The average interpolation error in geocoding can be characterized as ± one-half the length of a block, which corresponds to 75–140 m for large arterial and local roads in the urban areas, and 100–200 m for roads in the rural areas, respectively.

A GIS-based processing scheme was developed to transfer the Caltrans vehicle activity information onto the TAMN road network database. An automated GIS algorithm was developed, which outputs a relational cross-reference file that matches Caltrans road links (with

vehicle activity and fleet composition) to the corresponding TAMN road segments. The transferring of the Caltrans annual average daily traffic (AADT) counts to the TAMN database yielded a match rate exceeding 95%. The unmatched pairs were mostly due to name mismatches (e.g. misspelling in the names) or large discrepancies in the geometry of roadway links (e.g. a link shown in Caltrans roadway network might not exist in the TAMN network). Manual matching was applied to facilitate assigning the unmatched Caltrans links to the TAMN data, especially in cases where street names were misspelled.

CALINE4 model sensitivity runs were conducted under different meteorology conditions and receptor locations. For a simple case of light daytime winds (2 m/s, with slightly unstable atmospheric conditions) blowing perpendicular to a busy, at-grade freeway (10,000 vehicles per hour), the CALINE4 model estimated a factor of eight difference in the concentrations of carbon monoxide at receptors located 30 m and 300 m downwind of the roadway centerline. Using a single line to represent a freeway (in Caltrans data) or double lines for two directions of a freeway (in TAMN data) can also result in different pollutant concentration estimates. The CALINE4 sensitivity test showed that a two-direction freeway scenario resulted in pollutant concentrations 30% lower than a single freeway scenario at a receptor 30 m downwind of the freeway.

Conclusion. This study demonstrated that large discrepancies, up to hundreds of meters, may exist among different roadway network data. Relative misplacements of roadways and participant locations of this magnitude can lead to significant misclassification of exposure estimates, up to an order of magnitude in vehicle-exhaust pollutant concentrations. Studies concerned with human exposure to air pollutants adjacent to roadways must account for such discrepancies. We successfully developed and applied a GIS method to address this problem (Wu, et al., 2005b).

Environmental Justice and Traffic-Related Air Pollution in Southern California

Objectives. Health studies showed that residents of inner-city, minority, or low-income areas were at higher risk for chronic respiratory disease because of air pollution (Eggleston, et al., 1999; Mann, 2000; Weiss, et al., 1992). Documenting and quantifying the distribution of traffic density in southern California is an essential step and prerequisite to understanding potential exposure patterns and in formulating policy and planning interventions that can help minimize the hazardous impact of vehicle-related pollutants for all residents. The objectives of this research were to identify the geographic pattern of race and poverty in southern California; document the overlap of disadvantaged neighborhoods and the transportation network; and quantify the potential disparities in traffic volume by neighborhood type.

Project Summary. Race and ethnic population data were obtained from Census 2000. The distribution of parcels by residential type (single family and multifamily) was derived from the Statewide Database of the University of California at Berkeley. Vehicle activity data for southern California were obtained from the California Department of Transportation. Neighborhood measures and traffic volume for block groups were aggregated in five southern California counties (Los Angeles, Orange, Riverside, Ventura, and San Bernardino), and by two race-based classifications (Minority and Non-Minority) and four poverty-based classifications

(Very Poor, Poor, Low Poverty, and Not Poor). Block groups with over 40% of residents in poverty were classified as "Very Poor".

Based on 2000 census data, the Los Angeles–Long Beach Metropolitan Statistical Area had a Dissimilarity Index score of 67 for African Americans, indicating that that 67% of African Americans in that metropolitan area would have to move in order to be evenly distributed among Non-Hispanic Whites in the region. Patterns of racial segregation were closely intertwined with the persistence of concentrated poverty in southern California. Between 73–86% of poor residents would have to relocate within the region in order to be evenly distributed among the non-poor in the region. Although certain neighborhoods with predominately minority populations were in outlying areas, most were located in the densely populated urban core of the region, particularly in areas near downtown Los Angeles and South Los Angeles.

The separation of residents based on race and income functionally divided residents spatially based on a number of related socioeconomic characteristics. Residents of minority and very poor had lower levels of educational attainment. The very poor areas were 92 percent Non-White, and 61 percent of residents had less than a high school education. These areas also had lower rates of labor force participation. Whereas 81 percent of working age residents of non-minority neighborhoods were in the labor force, only 68 percent of working age residents of minority areas participated in the labor force. This rate was even lower in very poor neighborhoods. Minority and poor areas had a higher population density and a higher prevalence of multifamily residential parcels and older buildings than the remainder of the region. Whereas only 18% of residential parcels in minority areas were multifamily, 32% and 48% were multifamily in poor and very poor areas, respectively. Residents of disadvantaged areas also had fewer transportation resources. Whereas approximately 95% of households in non-minority areas have a household vehicle, only 86% in minority areas had a vehicle. Eighty-one percent or fewer had access to a vehicle in poor and very poor areas, compared to 96% in not poor neighborhoods. Furthermore, a lower percentage of workers traveled to work by auto in disadvantaged neighborhoods while a higher percentage traveled by public transportation.

We found that the road density of very poor areas was almost two times that of the least poor neighborhoods. Minority areas have almost 2.5 times the traffic density of non-minority areas. Very poor areas, which represent the most disadvantaged areas in the region, had a significantly higher traffic density than minority or poor areas, perhaps because these areas have the highest roadway density. Given the magnitude of the disparities in the distribution of traffic by these neighborhoods, there is reason to suspect that residents of minority and poor areas are at a higher risk of the health effects associated with vehicle-related pollutants.

Almost half (44%–47%) of vehicle miles traveled (VMT) in the study region were on major roads as compared to highways, indicating that the adverse effects of traffic density are spread across the urban roadway system and not confined to highways. The distinction of traffic levels between major roads and highways was even more pronounced for high-density areas. While less than 40% of VMT was on major roads in the lowest density areas, 56% of VMT was on major roads in areas of the region's highest density. Clearly, non-highway arterials played a major role in sub-regional traffic patterns and should be included in future research.

Conclusion. Disparities in local traffic patterns in southern California were embedded within regional social and economic forces. Minority and high-poverty neighborhoods were distinct from other areas in the region. In aggregate, they had a higher population density, lower housing values and a high density of highways and major roads. These neighborhoods bear over two times the level of traffic density compared to rest of the region. Furthermore, they have older and more multifamily housing, which is associated with higher air exchange rates or higher indoor exposure to outdoor pollutants.

Airshed Modeling

Objective. Modeling the distributions of particle-borne materials and gaseous pollutants across the LAB is crucial for assessing the health impacts of emissions on the regional population of the LAB. It is especially important for sparsely measured, but critically important, components of smog such as elemental carbon, polycyclic hydrocarbons and their photochemical byproducts, trace metals, peroxides, and other suspicious substances. Results from model simulations are useful for characterizing the spatial and temporal variations and sources of agents of interest to the SCPCS health research team, and therefore contribute to the regulatory role of the EPA and other agencies.

The principal objective of the airshed modeling was to provide modeling support for several of the projects in the SCPCS, including the exposure assessments for the CHS. The SMOG airshed model was used to determine background pollutant abundances used in detailed CALINE4 model calculations, yielding more accurate and comprehensive evaluations of long-term average exposures of the individual CHS children to vehicle-related pollutants.

A second objective was to establish the regional distributions of pollutants for population exposure assessments with the REHEX code. Toward this end, a focused LAB scale assessment of naphthalene and its photochemical byproducts, the naphthoquinones, was undertaken. It turns out that there has been remarkably little work done on these compounds. Importantly, naphthalene is presently receiving greater attention due to its potential carcinogenic nature.

UF are suspected as causative agents for a wide range of adverse health outcomes including morbidity and mortality. Traffic from freeways and local roadways contribute to UF concentrations in adjacent communities. We have also initiated detailed modeling of UF size distributions for freeway exposure studies.

Project Summary and Accomplishments. Progress was made in a number of areas, including the modeling of distributions of particle-borne materials and gaseous pollutants across the LAB, the assessment of the regional distributions of and human exposure to naphthalene and naphthoquinones in the LAB, application of the SMOG model in support of the CHS, and development of a detailed model for UF size distributions for freeway exposure studies.

The Surface Meteorology and Ozone Generation (SMOG) Airshed Model. Over the past decade, we have developed a model that can be used to predict the distributions of gaseous and particle-borne pollutants across the LAB (Figure 3). Previous work has established the capabilities of the SMOG model through comparisons of model simulations against observations (e.g., Jacobson, 1997; Jacobson, et al., 1996; Lu and Turco, 1996, 1997; Lu, et al., 1997a; 1997b; Lu, et al., 2003; 2005). The components of the SMOG modeling system are shown schematically in Figure 3 and are discussed in detail in the references provided. The specific information required for the naphthalene simulations is discussed below.

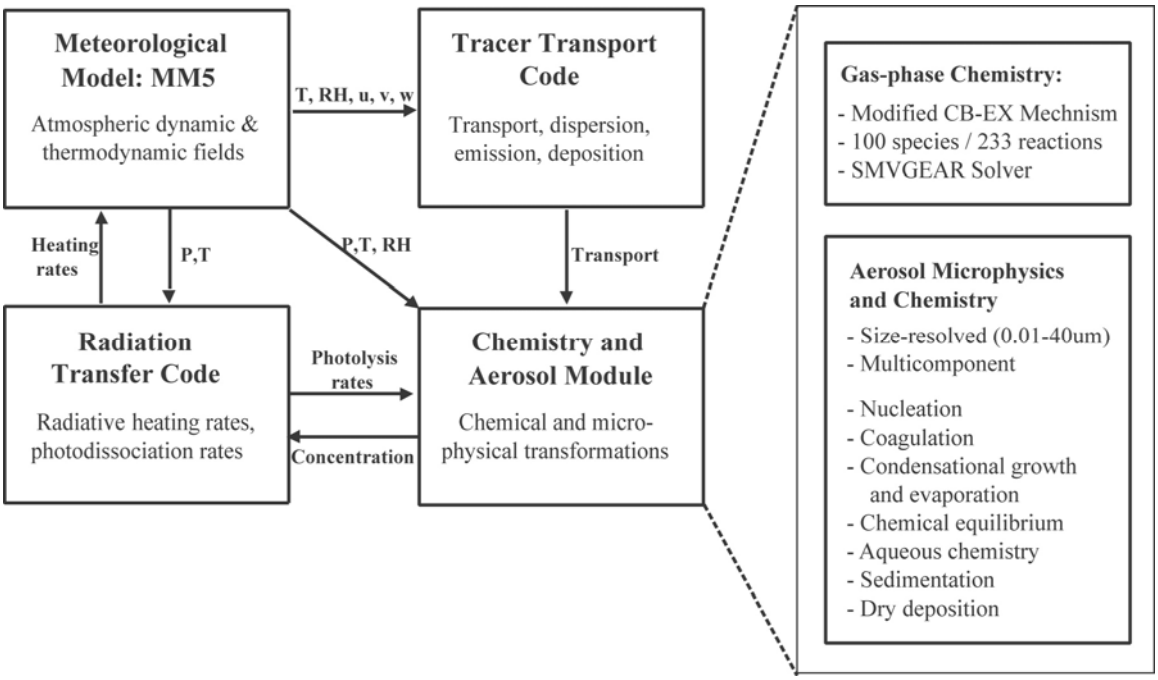

Figure 3. The SMOG Modeling System. The meteorological predictions are currently carried out using a triple-nested version of the mesoscale model (MM5) with initialization based on National Center for Environmental Prediction global data.

The regional primary pollutant emissions fluxes, photochemical reaction coefficients, and dispersion rates have been reported previously (Jacobson et al., 1996; Lu et al., 1997a). In assessing the fidelity of the SMOG model, the largest uncertainties arise from errors in the emission rates and patterns that are available from standard sources. Refinements to mobile emissions (e.g., for reactive hydrocarbons) based on suggestions from literature has been incorporated into simulations, as described and evaluated by Lu et al. (1997a; 1997b). In this study, the Air Quality Management District (AQMD) 1998 emission inventory has been used. The result is overall statistical agreement between model predictions and monitoring data for criteria pollutants in the range of +25–35%, with larger variability for particulates in general. In addition to emission refinements, we can also perform inverse modeling to calibrate total emissions in cases where the sources are inadequately identified or quantified. This approach is described elsewhere (Lu et al., 2003). Calibration of simulations against observations is effective in limiting biases in the predictions.

Results suggest that, in estimating human exposure to airborne pollutants, and setting standards for exposure, crucial information can be provided by regional modeling that would otherwise be difficult to obtain using ground-based measurements alone. At the same time, the distributions of co-pollutants can be obtained in a self-consistent manner.

Regional Distributions and Behavior of Particulate-Borne Trace Metals in the LAB

Trace Metal Distributions. In preliminary work to establish the capabilities of the SMOG model in simulating airborne particles and their composition throughout the LAB, we carried out the first detailed analysis of aerosol trace metals in the region, including sources, microphysical processing, meteorological dispersion, sedimentation and deposition, and ventilation from the LAB (Lu et al., 2003).

Figure 4 illustrates the predicted surface concentrations of zinc in total suspended particulates (TSP) over the LAB on a typical summer day corresponding to a recent sampling campaign. The distributions of trace metals (more than a dozen are available for analysis) are found to exhibit characteristic patterns across the LAB, which are similar to the pattern for PM_{10}. The model predictions have been checked by comparison to simultaneous PM filter samples at multiple sites (Multiple Air Toxics Exposure Study, MATES II). However, there are significant variations between the patterns for different metals. Importantly, different metals are found to be concentrated in different particle size ranges (Zn tends to lie within the larger particle fraction, for example). Our work demonstrates that the SMOG model reproduces these key properties of the trace metal distributions.

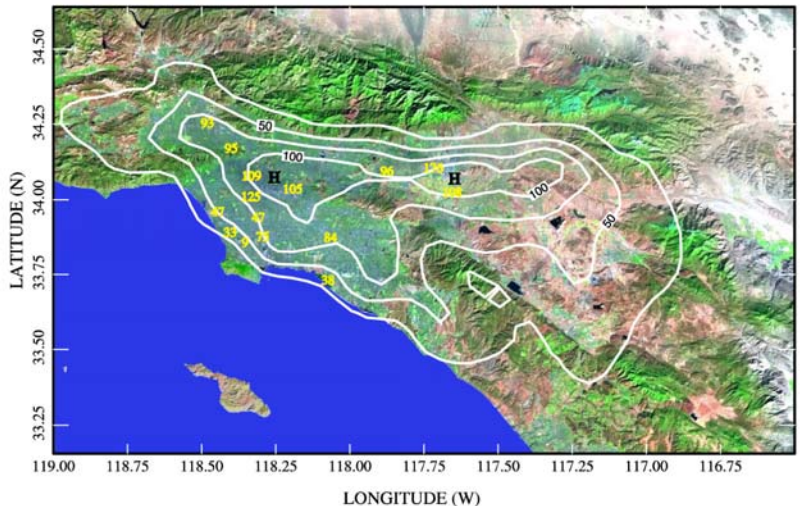

Figure 4. Comparison of SMOG-Predicted Zn Abundances (Contours) With Site Measurements (Yellow Numbers) in Nanograms per Cubic Meter (ng/m^3)
The contours represent 24-hour average total particulate Zn concentrations (at contour interval of 25 ng/m^3). The simulation corresponds to sampling periods during the MATES II project. The measured TSP (Zn concentrations) shown here are average values for the period July 1 to August 31, 1998.

Figure 5 shows the dramatic variations in the distributions of (and ultimately, exposure to) airborne particulates for different synoptic meteorological states characteristic of the LAB. Under Santa Ana wind conditions, for example, air is transported toward the southwest from the basin, forming a pool over the adjacent ocean surface. The particulate is deposited on the surface, or is advected to other coastal regions. Clearly, exposure to aerosols in the LAB is strongly influenced by meteorology as well as proximity to sources. These new results will allow us to combine tracer distributions corresponding to various synoptic states, using the statistical frequency of occurrence, to obtain more representative estimates of mean exposure, and to quantify more realistically extreme community-wide exposures encountered in the LAB.

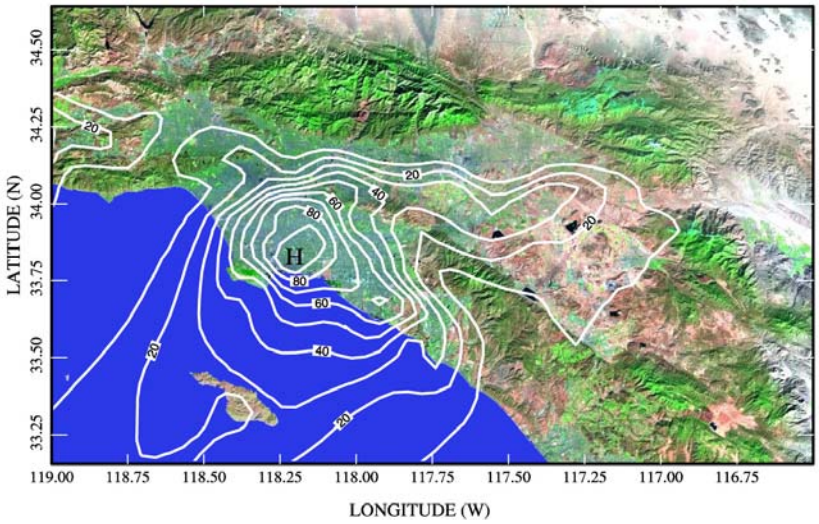

Figure 5. SMOG-Predictions of the Pb Distributions (Contours Give the Lead Abundance in ng/m^3) Across the LAB on a Day with Santa Ana Wind Conditions
The Pb contours extend over adjacent coastal waters in this case. The highest exposures would be expected to occur in the western areas of the LAB.

Results such as those in Figures 4 and 5 suggest that, in establishing exposure standards, crucial information can be provided by a regional model that would otherwise be difficult to obtain using ground-based measurements alone. Likewise, synergy between simulation and observation exists in the essential need for data to calibrate models (see below), and to define variability associated with local sources. Regional scale predictions complement site measurements by offering greater time resolution, and explicitly defining diurnal variations in surface concentrations of PM components (whereas 24-hr averaging is more typical in measuring particulates). Thus, for example, exposure at different times of the day can be reasonably estimated using modeled pollutant behavior. Finally, the distributions of co-pollutants are also available from simulations. The analysis for zinc and lead shown in Figures 4 and 5 has been extended to other aerosol trace metals, and is now available for different seasons and synoptic conditions (Lu, et al., 2003).

Calibrating Regional Simulations. We have evaluated and calibrated the emissions of particulate-borne trace metals using model simulations contrasted against regional monitoring data. In the past, this approach has been applied to calibrate volatile organic compound (VOC) emissions (Lu, et al., 1997a; 1997b). The burden of a particulate trace metal is determined as a balance between its integrated area-wide emission, subsequent meteorological dispersion, and eventual removal by deposition and ventilation. Figure 6 shows correlations of predicted and measured surface concentrations of zinc at 15 sampling sites during July and August 1998. In the SMOG calculations, we initially used emissions quantified by California Air Resources Board (CARB) in 1998. This led to a mean bias in the predictions that was subsequently used to calibrate—in a regional average sense—the local community-scale emissions (Lu, et al., 2003).

The calibration factor is calculated as the normalized bias between predictions and observations. This analysis reveals that a single adjustment to the emissions on a regional scale is capable of bringing simulations and observations into excellent accord—with less than 20% residual mean variance (at least for the sites where data were available, and for a sample averaging time of 24 hours).

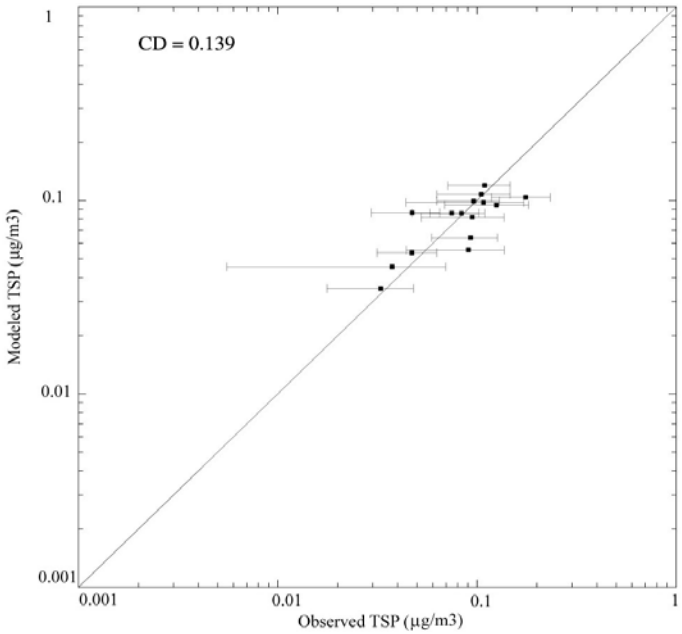

Figure 6.

Properties of Diesel Exhaust in the LAB: Elemental Carbon Sources and Distributions

The SMOG model was used to calculate and analyze the spatial distribution, size dispersion, and temporal behavior of elemental carbon (EC) in the LAB. Emission estimates for EC are available from the AQMD and ARB. We also have access to emission data on smoke aerosol components from firewood, cooking and other activities as previously compiled by center investigator Glen Cass and his collaborators. A similar approach to that used to calibrate trace metal emissions can be applied to constrain the sources of other essentially inert materials, such as elemental carbon. The overall EC emissions in the LAB have never been tested in this way. Rather, many individual sources have been identified, and each has been quantified independently. This is where the particle instrument unit (PIU) and other SCPCS observations are proving to be highly supportive of the modeling effort as we construct a more accurate regional emissions database for use in exposure assessments.

EC is treated as an unreactive tracer on the time scales of interest—that is, during dispersion and deposition throughout the LAB. A typical simulation of the EC distribution in the basin is given in Figure 7. The average distributions are obviously strongly influenced by sources along freeway corridors, noticeably along the 10 freeway in the northern and eastern basin, the 5/405

convergence in the northern San Fernando Valley, and along the Alameda corridor. The corresponding calculated mean size distribution of the elemental carbon component of the particulate shows peak abundances (by mass loading) in the UF below about one μm diameter, and in the large particle mode near 10 μm. The former peak is clearly associated with diesel exhaust, while the latter is an artifact of tire wear and road dust resuspension, and is more concentrated near freeways (note that tire rubber is treated as EC in the standard inventories).

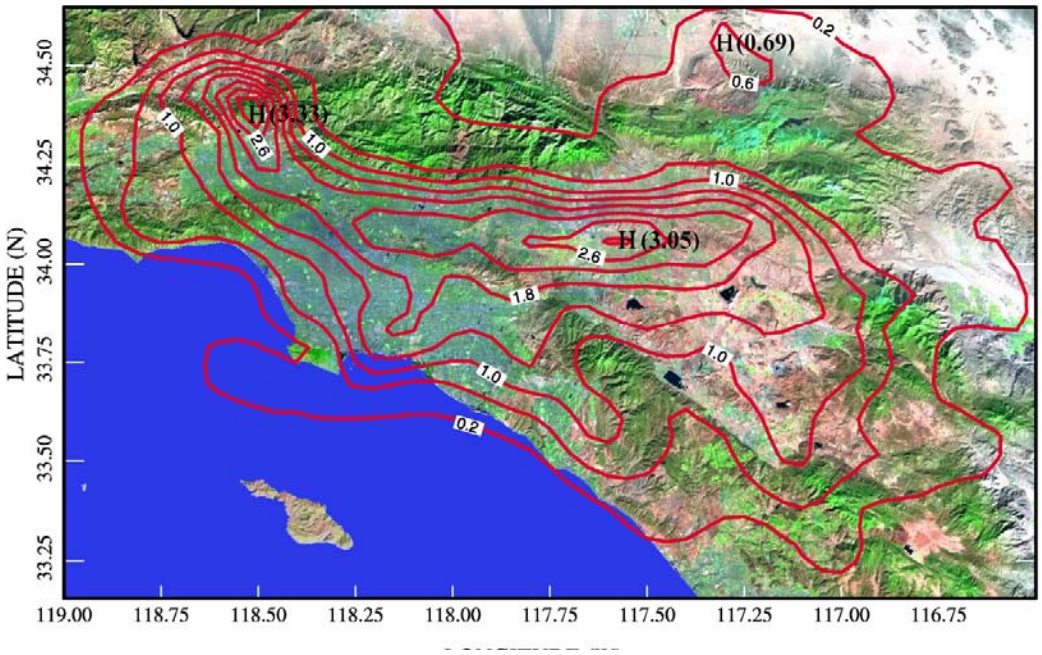

Figure 7. Distribution of Elemental (Black) Carbon, or Soot, Predicted for a Typical Summer Day

The abundances (in micrograms per cubic meter, μg/m^3) shown represent 24-hour averages. The predicted concentrations are consistent with EC data collected by the AQM

The SMOG model can be employed to resolve explicitly the temporal, spatial, and size variations associated with each distinct source of elemental carbon (e.g., diesel vehicles, stationary sources, tires, and so on). This offers the SCPCS a comprehensive characterization of such particulates for health impact assessment. Importantly, the implications of changes in specific sources can be quantified once the SMOG model is fully calibrated against SCPCS and other field measurements.

Distributions of Naphthalene and Its Derivative Quinones in the LAB

Naphthalene is the simplest and most abundant of the PAHs, organic compounds with at least two aromatic rings fused together (Arey, et al., 1989). Although PAHs with four rings or greater are found predominately in the particulate phase, as a double-ringed PAH, naphthalene in air occurs primarily in the gas-phase and has been detected in both outdoor and indoor samples. Naphthoquinones are photooxidation byproducts of naphthalene (Atkinson, et al., 1987; Sasaki et al., 1997). The potential health effects of exposure to quinones are a current focus of research.

Quinones express their toxicity through both electrophilic addition and oxidation-reduction reactions. One equivalent of quinone can generate multiple equivalents of reactive oxygen species and thus overwhelm the protective effects of antioxidant enzymes and other reducing agents (Nel, et al., 2001; Li, et al., 2000).

Naphthalene is a blood toxicant. Exposure to high concentrations of naphthalene can damage or destroy red blood cells, causing hemolytic anemia (USEPA, 2002). Naphthalene fumes can irritate eyes, skin and the respiratory tract. If inhaled over a long period of time, naphthalene may cause kidney and liver damage, skin allergy and dermatitis, cataracts and retinal damage, as well as attack the central nervous system. In animal tests, naphthalene has caused cancer as a result of inhalation (USEPA, 2002).

The regional distributions of PAHs such as naphthalene, and the formation of secondary organic compounds like the quinones and nitro-PAHs, are largely uncharacterized in the LAB. It is becoming apparent that naphthalene and its byproducts represent potential human health hazards. Naphthalene is rarely measured except in local sampling projects, and usually for limited periods. Here, the SMOG model is employed to depict the distributions of these species in much more detail than can be inferred from existing measurements alone.

Naphthalene Photochemistry. Using SMOG, we calculate the ambient abundances of these compounds based on the simplified photochemical scheme in Figure 8. The concentration of naphthalene is controlled by its reactions with the hydroxyl radical, OH, and with the nitrate radical, NO_3. Of these two reaction pathways, the OH process is more important. The concentrations of naphthalene and its immediate byproducts are largely controlled by reactions with the hydroxyl radical. The key reaction in the decomposition of naphthalene involves OH addition, for which the rate constant is known ($\sim 2.4 \times 10^{-11}$ cm^3/s at 298 K). Naphthalene also reacts with nitrate radicals, although this path is most effective at night. In the presence of NO, the yield of naphthoquinones and related species via the OH reaction can be as large as ~40%, depending on the number of compounds counted in this reactive cohort. The direct yield of 1,4-naphthoquinone is roughly 1%. Atkinson and Arey (private communication, 2001). A roadmap for the secondary reactions of several of the naphthalene products with OH has been constructed using specific laboratory measurements as well as analogous organic chemical processes. As a result, the distributions of naphthalene and its principal secondary quinone-like products can be reasonably estimated.

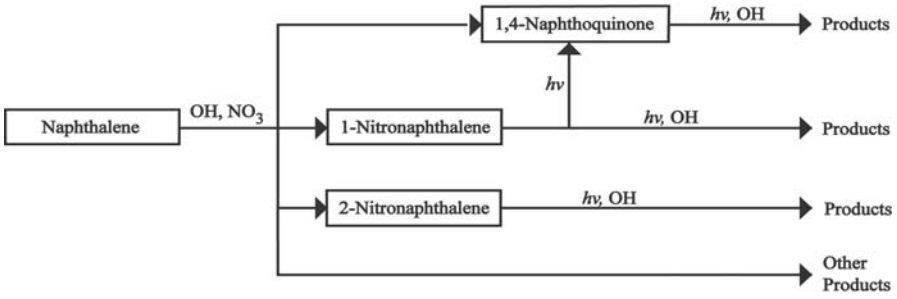

Figure 8. The Photochemical Oxidation Pathways Used to Determine the Ambient Abundances of Naphthalene and Its Quinone-Like Reaction Products

The balance for naphthalene is maintained between emissions (and dispersion) and reactions (mainly with OH). Thus, it is a simple matter to keep track of the naphthalene burden using an airshed model with a detailed photochemical mechanism (e.g., Lu, et al., 1997b). The decomposition reactions represent the sources of the quinones. The loss rates of the naphthoquinones are also dominated by OH. Hence, these products can also be tracked explicitly using SMOG simulations.

We note that naphthalene and its immediate photochemical products exist mainly in the vapor phase. Nevertheless, the product naphthoquinone and nitroquinones have lower vapor pressures and are partially partitioned onto particles. The SMOG model determines the total quantity of each compound in air, including the vapor and aerosols phases. To carry out a more thorough assessment for naphthalene-related organic compounds, physicochemical properties such as vapor pressures and solubilities must be incorporated into the modeling. For naphthalene and many other common PAHs, and their stable photochemical products, relevant data are available to determine vapor/particle partitioning factors.

Validation of Naphthalene Emission Rates. Uncertainties exist in mobile source emission factors for naphthalene, in part due to sampling difficulties. For example, naphthalene can be lost to walls when exhaust gases are collected and stored in bags. Since naphthalene is too volatile for complete collection on a denuder, it is also necessary to back up denuders with polyurethane foam (PUF) cartridges. In addition, mobile source emission factors are usually determined by sampling exhaust from a small number of vehicles under conditions that may not be representative of vehicles in use.

In contrast, benzene can be reliably measured in both vehicle exhaust and ambient air, and the ratio of naphthalene to benzene may be used to assess the reliability of naphthalene emission factors. Hence, to verify mobile source emission factors for naphthalene, we conducted a sampling experiment at the Sepulveda tunnel near the Los Angeles International Airport (LAX) with high traffic volume. The overall average naphthalene-to-benzene mass ratio determined for the tunnel samples is identical to the ratio corresponding to averaged gasoline vehicle emissions based on the ARB emissions inventory. Accordingly, the tunnel results provide strong support for the naphthalene emission rates used in the air quality simulations.

To further verify emission factors using the ratio technique, ambient air samples were collected at the California Institute of Technology, Pasadena CA, roughly 20 km northeast of downtown Los Angeles. This area is subject to light and heavy-duty vehicle traffic, as well as point and area sources of naphthalene. The naphthalene-to-benzene mass ratios for the 24-hour samples are consistent with the naphthalene-to-benzene mass ratio predicted by the SMOG model. Since benzene is emitted mainly from mobile sources, the agreement between the modeled and measured naphthalene-to-benzene ratios indicates the relative contributions to the total naphthalene emissions from mobile sources together with other sources are represented reasonably well in the emission inventory employed here.

Naphthalene Distributions Across Southern California. Figure 9 illustrates the predicted summer concentrations of naphthalene across Southern California. The regional character of the naphthalene distribution is clearly revealed with high concentrations confined largely within the basin defined by mountain ranges to the north and east and coastal ocean to the west and south. Large naphthalene gradients occur along the coast owing to prevailing winds, which transport polluted air masses inland. The peak naphthalene concentrations appear in areas where emissions are greatest; for example, adjacent to downtown Los Angeles. Winter concentrations, on average, exceed those in summer.

Naphthalene emissions are associated with fuel combustion and vaporization. Accordingly, the predicted distributions correlate strongly with transportation corridors in Southern California. For example, high concentrations stretch along the San Gabriel and San Bernardino Mountains in the northern and eastern basin corresponding to the 10 and 210 freeway corridors. Another band of high concentrations extends southeast between the San Fernando Valley and Orange County paralleling the 5 and 405 freeways. Atmospheric dispersion from sources also plays a critical role in controlling the regional distribution of naphthalene, leading to the widespread distributions noted in Figure 9. The high degree of spatial variability suggests one needs a multi-station network like those used to characterize ozone and NO_2 in Southern California to properly characterize naphthalene (and other PAHs) in urbanized regions.

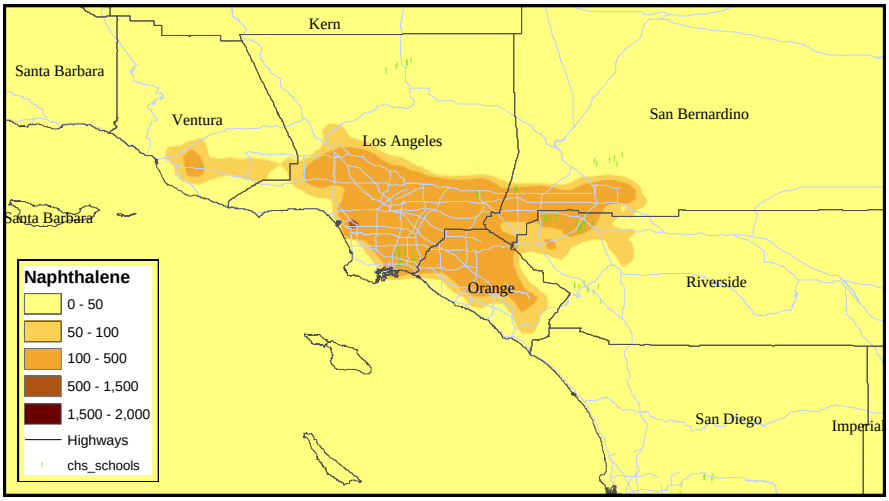

Figure 9. Predicted Distributions of Naphthalene Across the LAB Corresponding to 1998 Summer Emissions (in Units of ng/m^3)

The distribution of 1,4-naphthoquinone in both gaseous and aerosol phases generated by naphthalene photooxidation is shown in Figure 10. Significant differences can be seen between the concentration patterns of the primary and secondary compounds—naphthalene and naphthoquinone. The 1,4-naphthoquinone is concentrated inland along the mountain slopes where air trajectories arrive from the coastal region.

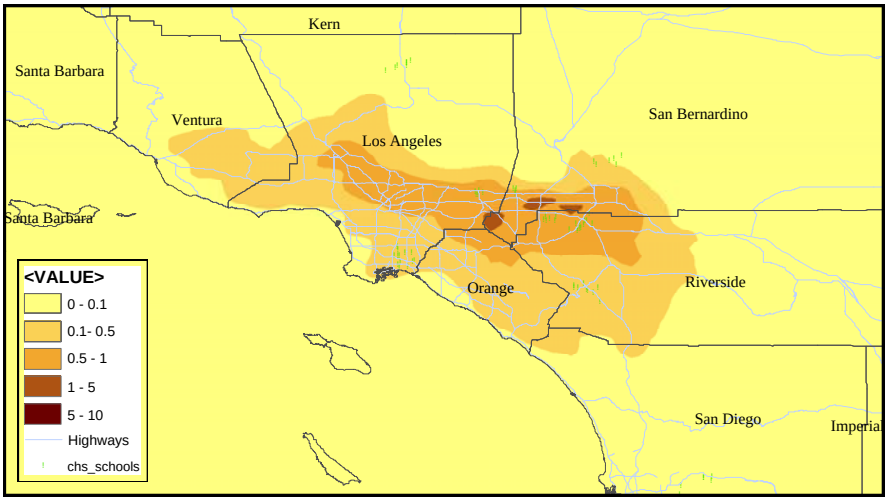

Figure 10. Concentration Contours for the 1,4 Naphthoquinone Byproduct of Naphthalene (in Units of ng/m^3)

In this analysis, 1,4-naphthoquinone concentrations are from photochemical production only. However, other processes not accounted for in this analysis may also contribute to the total

burden. For example, the photo-transformation of naphthalene on solid surfaces and fly ash apparently generates naphthoquinones (Guillard, et al., 1993). Similar processes may occur on aerosol surfaces in polluted airsheds. Bunce, et al. (1997) noted the formation of naphthoquinones in the reaction of naphthalene with OH radicals and subsequent secondary reactions with a peak yield of 6% under their experimental conditions. Moreover, quinones may be emitted in vehicle exhaust (Choudhury, 1982). Further, the toxicities and health impacts of naphthalene oxidation products other than naphthoquinone, including naphthols, formylcinnaldehyde, and certain dicarbonyls, are largely unknown. The yield of each of these compounds from the oxidation of naphthalene ranges between ~3% and 35% (Sasaki, et al., 1997). It follows that the sum of these additional compounds could significantly exceed the predicted concentrations of 1,4-naphthoquinone based on the photochemical scheme in Figure 8. Further work is required to quantify the abundances of quinones in urban air, and to characterize their regional distributions and human exposure.

In the case of naphthalene, simulations and observations are in relatively good agreement. This implies that the total emission inventory may be within the range of a factor of 2. However, uncertainties about specific sources are larger, especially from mobile sources and fuel leakages. The demonstrated existence of distinct distribution patterns for the parent species and its secondary compounds (e.g., comparing Figures 9 and 10) implies distinct chemical "fingerprints"—consisting of combinations of spatial patterns and ratios of concentrations—that could be exploited to identify the contributions from individual sources (e.g., gasoline vaporization). This requires more detailed measurements, however, and cannot be pursued at this time.

Naphthalene Exposure Assessment with the REHEX Model. The naphthalene concentration estimates obtained from the SMOG model are employed in the REHEX model to calculate population exposure statistics. Results show average hourly naphthalene exposures in Southern California under summer and winter conditions of 270 ng m^{-3} and 430 ng m^{-3}, respectively. Exposure to significantly higher concentrations may occur for individuals close to local sources, or in naphthalene "hotspots" revealed by simulations and observations. Such levels of naphthalene exposure may be used to gauge the potential health impacts of long-term naphthalene exposure. Results are also given for the distributions of 1,4-naphthoquinone, a naphthalene reaction product that may have significant health effects.

Application of the SMOG Model in Support of the SCPCS CHS

We have continued to improve and apply the SMOG model calculations to support the SCPCS CHS analysis being carried out by Winer, Lurmann and Wu, as summarized in the exposure modeling section of the report. New sources of emissions data have been incorporated in as a means of improving the overall reliability of the air quality and exposure calculations. The airshed model predictions provided background pollutant concentrations to estimate the exposure of individuals based on an analysis with the personal exposure model, IEM.

Updated Emission Inventories. To improve the predictions of particulate pollutant distributions for exposure assessment in the SoCAB, we updated primary emission inventories, incorporated a secondary organic aerosol (SOA) module, and integrated a biogenic emission database into the

SMOG model. The latest emission inventory developed for the AQMD 2003 Air Quality Management Plan (AQMP) was adopted to estimate CO, NOx, SOx, VOC and PM emissions in the SoCAB. The 2003 AQMP emission inventory treats point, area, off-road and on-road sources. The on-road emissions were estimated using the ARB EMFAC-2002 emission factors, and transportation activity data developed by the Southern California Association of Governments (SCAG) in their 2001 Regional Transportation Plan. Emissions from off-road vehicles, including trains, ships, construction equipment, and utility engines, were determined using estimated activity levels and emission factors for these sources. The revised inventory was spatially distributed over a grid system composed of 5-km by 5-km grid cells spanning Southern California. The incorporation of this database reduced uncertainties associated with the older "standard" emissions, which were based on inventories constructed in 1997. With the new emissions database, we have performed SMOG simulations for periods corresponding to specific SCPCS field campaigns, and compared SMOG predictions against these data to check the fidelity of the model with the latest emissions.

Secondary Organic Aerosol (SOA) Module and Biogenic Emissions. SOAs are an important component of the total particulate burden in the LAB, and many of the SOA constituents are semi-volatile. Hence, the SOA module tracks production of condensable gases formed during the oxidation of VOC precursors, calculates the equilibrium distribution between the gas and aerosol phase, and predicts changes in aerosol size distribution due to the condensation/evaporation process. Emissions of SOA precursors from biogenic sources contribute to the aerosol organic component. Biogenic emissions calculated using the ARB's BEIGIS model has been implemented in SMOG. BEIGIS is based on a California-specific input database with a minimum spatial resolution of 1 square km and hourly temporal resolution. The enhancements to the SMOG model described above have significantly improved our ability to model the distributions and organic composition of particulates and their precursors in the SoCAB.

CHS Simulations. The updated emission inventories also allow more reliable simulations of criteria pollutants of interest to the CHS supported by the SCPCS. Detailed baseline calculations of the background pollutant levels at CHS locales have been employed in the IEM (Wu, et al., 2005a), supported by the SCPCS for epidemiological evaluation of the CHS cohorts. A series of SMOG simulations for specific episode conditions have been provided to the IEM team, including a detailed quantification of the spatially resolved background abundances for use with theCALINE4 model. The exposure of individuals has been analyzed with the personal exposure model (IEM) with predictions of regional-scale gas and particle distributions and time variations associated with transported and local non-mobile sources corresponding to each of the CHS study areas. The SMOG background predictions for different seasons and sub-regions have been combined with roadway pollutant simulations with the CALINE4 model to provide the most detailed characterization to date of childhood exposure to air pollution in the SoCAB.

<u>Modeling UF Near Major Roadways for Human Exposure Assessment</u>

UF are suspected as causative agents for a wide range of adverse health outcomes including morbidity and mortality. Due to the fact that they contribute very little mass to coarse particles (C) or fine particles (F), which EPA regulates, it is important to investigate UF properties and to

quantify their concentrations and human exposure. Although the U.S. EPA currently regulates total particle mass below 2.5 micrometers in diameter, UFs represent the smallest particles in this range, with the largest concentrations and potential health impacts. In fact, $PM_{2.5}$ mass is not really an indicator of UF properties. These concerns have led European agencies to contemplate regulating particles by number rather than by mass. Taking into account the potential health effects of the UF and the fact that they contribute very little to C or F, it is important to investigate their properties and to quantify their concentrations and human exposure.

We developed and applied new modeling tools to characterize UF near major roadways. A new microphyical analytical parameterization in addition to the comprehensive microphysical treatment in SMOG were utilized. Field-measurement datasets were employed to test and validate model predictions near roadways. The CALINE 4 roadway line source code was used to achieve high spatial resolution. The emission rates of UFs from major roadways were estimated from field measurements and traffic counts of gasoline and diesel vehicles. A box-version of the SMOG air pollution model (Lu, et al., 1997a) with an explicit treatment of coagulation, condensation/evaporation, deposition, as well as dilution processes, was used to simulate the evolution of UFs as they move downwind from selected roadways. Preliminary simulations indicated that the model reproduced the main observed features of UF transformations near freeways. These detailed simulations also revealed the primary transformation processes that control UF number concentration and size distribution. These insights guided the development of a simplified UF analytical model that is practical for human exposure assessment applications.

Analytical solutions of the equations describing aerosol coagulation and vapor condensation in an expanding plume have previously been derived and used to simulate aerosol plumes from aircraft emissions (Turco and Yu, 1998; 1999). Similar techniques were adapted here to study freeway line sources of interest (e.g., Figure 11). The analytical roadway UF model accounts for the coagulation and condensational growth of a size distribution of aerosols from a specified source. The condensation processes that can be accounted for include volume condensation (or bulk reaction controlled uptake), surface-controlled condensation (typically applicable to very small particles), and diffusion-limited condensation (for larger particles). The UF parameterization yields the properties of UF evolving in traffic line emission plumes. The expansion rates of such plumes were calculated using measured (or in some cases predicted) CO concentrations. With initial UF number and mass concentrations, as well as estimates of the concentrations of condensing vapors, the particle number concentration and size distribution at downwind receptor points could be calculated. The simple UF model has been coupled with the CALINE 4 roadway line source model to determine UF distributions near major roadways due to vehicle emissions (Figure 11).

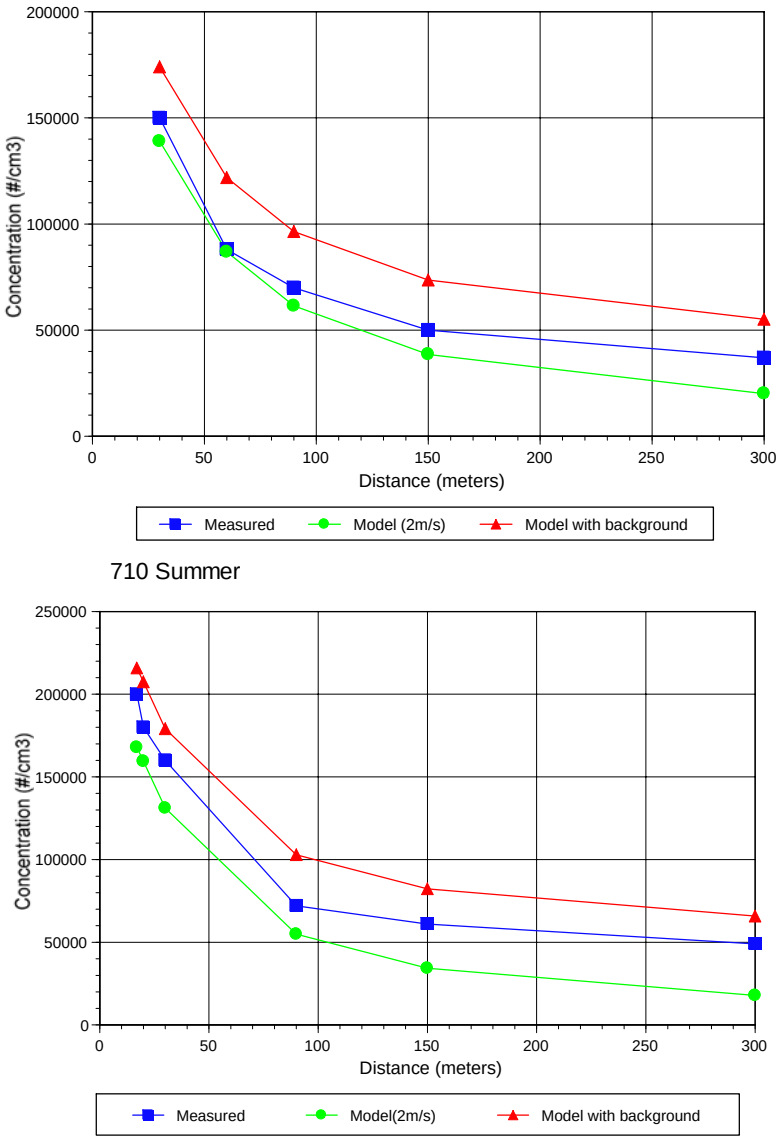

Figure 11. Comparisons of Observed (blue symbols) and Modeled UF Concentrations at the 405 and 710 Freeways

UF particle concentrations were predicted based on a microphysical parameterization in the CALINE 4 model (see the text). Circles and triangles show modeled concentration without and with background particles, respectively.

Motor vehicle exhaust is the major source of UF in urban environments. High particle number concentrations in the vicinity of freeways raise concerns regarding adverse health effects. However, field measurements show that UF number concentrations decline dramatically—and the corresponding size distribution changes rapidly—with increasing distance from major roadways (Zhu, et al., 2002a; 2002b; 2004). Comparisons of UF concentrations simulated with CALINE 4 and a UF parameterization are compared with measurements downwind of the 405 and 710 freeways in Los Angeles in Figure 11. The comparisons show that the modeling approach can provide useful information for exposure assessment under a variety of conditions that would be difficult to characterize observationally.

Conclusions

During the project period, significant accomplishments have been achieved in many areas, including the modeling of distributions of particle-borne materials and gaseous pollutants across the LAB, the assessment of the regional distributions of and human exposure to naphthalene and naphthoquinones in the LAB, application of the SMOG model in support of the CHS, and development of a detailed model for UF size distributions for freeway exposure studies. These achievements addressed the key National Research Council (NRC) research priorities of the use of advanced modeling to relate specific sources of PM to human exposure and the application of such models to connect toxicologically important constituents of PM to individuals and regional populations.

A new air quality and exposure modeling system, including a regional air quality model (SMOG), a local-scale line source model (CALINE4), an IEM and a population exposure model (REHEX), calculates individual or population exposures to vehicle-related pollutants by integrating pollutant concentrations in a variety of microenvironments, people's time-activity patterns, and ambient pollutant concentration estimates at different spatial resolutions (e.g. a point, tens of meters, or 5 km). This modeling system has facilitated analyses of exposure to local mobile emissions, non-mobile sources, and pollutants transported from upwind regions: these sources had not been investigated simultaneously and appropriately in previous studies. This advanced modeling system provides exposure assessment support for several projects conducted by the SCPCS and CHS, including the intra-community exposure variability analyses in the CHS study, the traffic density and emission assessment of the SCPCS, and investigation of exposure to species identified as of toxicological interest by SCPCS researchers. This system can also relate specific sources of pollutants to human exposure; quantify exposure of sub-populations that are potentially most susceptible to adverse health outcomes from PM-related pollution; create a linkage between the science resulting from the SCPCS/CHS programs and the policy and standard-setting goals established by the EPA; and aid in the design of cost-effective and optimally health-protective emission control strategies for F and particle-associated species.

References:

Arey J, Atkinson R, Zielinska B, McElroy PA. Diurnal concentrations of volatile polycyclic aromatic- hydrocarbons and nitroarenes during a photochemical air-pollution episode in Glendora, California. *Environmental Science & Technology* 1989;23(3):321-327.

Atkinson R, Arey J, Zielinska B, Aschmann SM. Kinetics and products of the gas-phase reactions of OH radicals and N2O5 with naphthalene and biphenyl. *Environmental Science & Technology* 1987;21(10):1014-1022.

Bunce NJ, Liu L, Zhu J, Lane DA. Reaction of naphthalene and its de-rivatives with hydroxyl radicals in the gas phase. *Environmental Science & Technology* 1997;31(8):2252-2259.

Choudhury DR. Characterization of polycyclic ketones and quinones in diesel emission particulates by gas chromatography/mass spectrometry. *Environmental Science & Technology* 1982;16:102-106.

Eggleston PA, Buckley TJ, Breysse PN, Wills-Karp M, Kleeberger SR, Jaakkola JJK. The environment and asthma in U.S. inner cities. *Environmental Health Perspectives* 1999;107(Suppl. 3):439-450.

Guillard C, Delprat H, Hoang-Van C, Pichat P. Laboratory study of the rates and products of the phototransformations of naphthalene adsorbed on samples of titanium dioxide, ferric oxide, muscovite, and fly ash. *Journal of Atmospheric Chemistry* 1993;16:47-59.

Hitchins J, Morawska L, Wolff L, Gilbert D. Concentration of submicrometer particles from vehicle emissions near a major road. *Atmospheric Environment* 2000;34:51-59.

Jacobson MZ. Development and application of a new air pollution modeling system. Part III: aerosol-phase simulations. *Atmospheric Environment* 1997;31:587-608.

Jacobson MZ, Lu R, Turco RP, Toon OB. Development and application of a new air pollution modeling system. Part I: gas-phase simulations. *Atmospheric Environment* 1996;30:1939-1963.

Li N, Venkatesan MI, Miguel A, Kaplan R, Gujuluva C, Alam J, Nel A. Induction of Heme Oxygenase-1 expression in macrophages by diesel exhaust particle chemicals and quinones via the antioxidant-responsive. *Journal of Immunology* 2000;165:3393-3401.

Lu R, Turco R. Ozone distributions over the Los Angeles basin: three-dimensional simulations with the SMOG model. *Atmospheric Environment* 1996;30:4155-4176.

Lu R, Turco R. An integrated air pollution modeling system: application to the Los Angeles basin. Numerical Simulations in the Environmental and Earth Sciences: In: Garcia F, Cisneros G, Fernandez-Eguiarte A, Alvarez A, eds. Proceedings of the Second UNAM-CRAY Supercomputing Conference. New York: Cambridge University Press, 1997, pp. 116-125.

Lu R, Turco R, Jacobson MZ. An integrated air pollution modeling system for urban and regional scales. 1. Structure and performance. *Journal of Geophysical Research* 1997a;102 (D5):6063-6079.

Lu R, Turco R, Jacobson MZ. An integrated air pollution modeling system for urban and regional scales. 2. Simulations for SCAQS 1987. *Journal of Geophysical Research* 1997b;102 (D5):6081-6098.

Lu R, Turco RP, Stolzenbach K, Friedlander SK, Xiong C, Schiff K, Wang G. Dry deposition of airborne trace metals on the Los Angeles Basin and adjacent coastal waters. *Journal of Geophysical Research* 2003;108(D2): 4074.

Lu R, Wu J, Turco R, Winer A, Atkinson R, Arey J, Paulson S, Lurmann F, Miguel A, Eiguren-Fernandez A. Naphthalene distributions and human exposure in the South Coast Air Basin. *Atmospheric Environment* 2005;39:489-507.

Mann J. Asthma in San Francisco. Community Health Epidemiology and Disease Control, San Francisco Department of Public Health, 2000.

Nel AE, Diaz-Sanchez D, Li N. The role of particulate pollutants in pulmonary inflammation and asthma: evidence for the involvement of organic chemicals and oxidative stress. *Current Opinion in Pulmonary Medicine* 2001;7:20-26.

Sasaki J, Aschmann SM, Kwok ESC, Atkinson R, Arey J. Products of the gas-phase OH and NO3 radical-initiated reactions of naphthalene. *Environmental Science & Technology* 1997;31(11):3173-3179.

Turco RP, Yu F. Aerosol size distribution in a coagulating plume: analytical behavior and modeling applications. *Geophysical Research Letters* 1998;25:927-930.

Turco RP, Yu F. Particle size distributions in an expanding plume undergoing simultaneous coagulation and condensation. *Journal of Geophysical Research* 1999;104(19):227-241.

USEPA. Health Effects Support Document for Naphthalene. EPA 822-R-02-031, Office of Water, Health and Ecological Criteria Division, Washington, DC, 2002.

Weiss KB, Gergen PJ, Crain EF. Inner-city asthma: the epidemiology of an emerging U.S. public health concern. *Chest* 1992;106:362S-366S.

Wu J, Lurmann F, Winer AM, Lu R, Turco R, Funk T. Development of an individual exposure model for application to the Southern California Children's Health Study. *Atmospheric Environment* 2005a;39:259-273.

Wu J, Funk T, Lurmann F, Winer A. Improving spatial accuracy of roadway networks and geocoded addresses. *Transactions in GIS* 2005b;9(4):585-601.

Zhu Y, Hinds WC, Kim S, Sioutas C. Concentration and size distribution of ultrafine particles near a major highway. *Journal of the Air & Waste Management Association* 2002a;52:1032-1042.

Zhu Y, Hinds WC, Kim S, Shen S, Sioutas C. Study on ultrafine particles and other vehicular pollutants near a busy highway. *Atmospheric Environment* 2002b;36:4323-4335.

Zhu Y, Hinds WC, Shen S, Sioutas C. Seasonal trends of concentration and size distribution of ultrafine particles near major highways in Los Angeles. *Aerosol Science and Technology* 2004;38:5-13.

Supplemental Keywords: NA

Relevant Web Sites: http://www.scpcs.ucla.edu